


ORIGINAL RESEARCH PAPER

Enhancement of DC-bus voltage regulation in cascaded converter system by a new sensorless load current feedforward control scheme

Majid Ali¹  | Muhammad Yaqoob² | Lingling Cao³ | Ka-Hong Loo⁴
¹ Department of Electrical Engineering, Namal Institute Mianwali, Punjab, Pakistan

² Huawei Technologies, Sweden Research Center, Sweden

³ School of Mechanical Engineering and Automation, Harbin Institute of Technology, Shenzhen, China

⁴ Department of Electronic and Information Engineering, The Hong Kong Polytechnic University, Hung Hom, Hong Kong

Correspondence

Majid Ali, Department of Electrical Engineering, Namal Institute Mianwali, Punjab, Pakistan.
Email: majid.ali@connect.polyu.hk

Funding information

The Hong Kong Polytechnic University, Grant/Award Number: G-YBXL

Abstract

It is generally known that, with conventional PI control, the stability and dynamic response performances of a power converter cannot be optimized simultaneously. To overcome this limitation, an uncertainty and disturbance estimator assisted sensorless load current feedforward control for dc-bus voltage regulation is presented to achieve fast dynamic response to load variations while stability is guaranteed by tuning PI controller. The proposed control scheme is verified on a cascaded converters system comprising a front end dc-dc DAB converter followed by a single-phase inverter as an illustrative case. Load-current feedforward is used to enhance the transient response of the front end DAB converter while an uncertainty and disturbance estimator is used to compensate for any non-idealities arising from model uncertainties and error in load current estimation. To validate the proposed control scheme, experimental results obtained from a 250-W cascaded converter system are presented and compared rigorously to the performance of conventional PI control.

1 | INTRODUCTION

Back-to-back converters comprising a front-end dc-dc converter followed by an inverter are commonly used in applications such as uninterruptible power supplies (UPS), solid-state transformers (SST), grid-integrated energy storage systems and grid-integration of solar photovoltaic (PV) systems [1–4]. Dual-active-bridge (DAB) dc-dc converter is gaining more and more attraction in these applications due to its bidirectional power-flow capability, soft-switching capability, high efficiency, and provision of galvanic isolation [5–7]. When the inverter is connected as a load to the DAB converter, there exists an ac-ripple component in the dc-bus voltage oscillating at twice the inverter's output frequency due to the pulsating instantaneous output power of the inverter. This double-line frequency ripple component can result in a reduced lifetime of the dc-bus capacitor and affects the inverter's output voltage quality. Therefore, it is necessary to minimize its amplitude in the dc-bus voltage.

Typically, a sizeable dc-bus capacitor is employed to reduce its magnitude, but this results in reduced power density and increased cost of the converter system [8–10].

For the regulation of dc-bus voltage, voltage-mode or current-mode PI controller are commonly used [11, 12]. However, the main drawback associated with PI control is that it is challenging for a PI controller to meet both dynamic response performance and stability requirements satisfactorily, as they are often in contradiction with each other. Hence, there is always a compromise between stability and transient response performance of the converter with this approach. Furthermore, variations in the converter's parameters and model uncertainties will adversely affect the performance of the conventional PI control method. Moreover, when the dc-bus voltage is regulated by using a PI controller, it cannot mitigate the second-order harmonic component in the dc-bus voltage without requiring a large capacitor. In the literature, various control methods are presented to enhance the transient response of the

This is an open access article under the terms of the [Creative Commons Attribution](https://creativecommons.org/licenses/by/4.0/) License, which permits use, distribution and reproduction in any medium, provided the original work is properly cited.

© 2021 The Authors. *IET Power Electronics* published by John Wiley & Sons Ltd on behalf of The Institution of Engineering and Technology

front-end DAB converter and to reduce the magnitude of the second-order harmonic component in the dc-bus voltage without increasing dc-bus capacitance [13–27].

To obtain an enhanced transient response, a lookup-table-based feedforward compensation scheme for the DAB converter has been proposed in [13]. In the proposed method, during each switching cycle, the load current is estimated based on the converter's parameters' nominal values and is used to obtain feedforward phase-shift from a lookup table and is added to the output of the PI controller. However, accurate knowledge of the converter's parameters is necessary for ensuring the effectiveness of the proposed method since any estimation error in the load current may result in discrepancies between the actual and desired phase-shift. Besides voltage-mode control, a current-mode control method with load current feedforward is proposed in [14]. In the proposed scheme, to obtain improved transient response performance, linear and non-linear load-current feedforward formulas are derived. They are used to add a feedforward term to the output of the PI controller. A boundary control method for the DAB converter is proposed in [15]. The natural voltage–current trajectories of the DAB converter are derived and used to produce the switching signals for the two active bridges. In [16], a digital predictive current-mode control is presented, where instead of sampling the actual average inductor current, which will require an analog-to-digital converter (ADC) with a high sampling rate. At the start of each switching cycle, the transformer current is sampled only once, and using the nominal values of the converter's parameters, the phase-shift required for the next switching cycle is calculated.

An asymmetric modulation scheme for DAB dc-dc converter is proposed in [17]. The required phase-shift values during transient events are distributed according to an optimized ratio between the primary and secondary bridges; this results in improved dynamic response and a reduced dc-bias in inductor current. To obtain an enhanced dynamic performance response in resonant dc-dc converters, a control law based on the Lyapunov method is derived [18]. In contrast to the conventional PI controller, the proposed method does not suffer from limited bandwidth limitation. In [19], the direct and quadrature components of DAB's converter inductor current are obtained by using a non-linear disturbance observer. Each of the inductor current components is then used to regulate the reactive and active powers of the DAB converter, respectively. To enhance the transient response performance of the DAB converter, a virtual direct power control method is proposed in [20]. In the proposed scheme, input/output voltages and the load current are sampled, and using this information, the required phase-shift is calculated and is added to the output of the PI controller. In [21], a unified-phase-control with power balancing strategy is proposed to improve efficiency and to enhance the DAB converter transient response. One major disadvantage common to both virtual direct power control and unified-phase-control with power balancing is that they require the use of extra voltage and current sensors.

To regulate the dc-bus voltage and effectively suppress the double-line frequency oscillation in the dc-bus voltage, a

proportional-integral-resonant (PI-R) controller is used in [22]. Two poles of the resonant controller are placed at the same frequency as the double-line frequency to achieve a high loop gain at that frequency. However, the addition of extra poles will increase the system order and may result in degraded dynamic response and reduced phase margin at other frequencies. A virtual impedance-based control method is proposed in [23] to reduce double-line frequency oscillation, where a band-pass filter is incorporated in the inductor current's feedback path to increase the impedance of the inductor current path. In [24] and [25], a dual-loop voltage-mode control method is proposed to shape the output impedance of the DAB dc-dc converter. Depending on the feedback gain selected for the inner voltage loop, the DAB converter will exhibit different closed-loop output-impedance characteristics. In [26], the dc-bus reference voltage is varied according to the load current so that the dc-bus capacitor nearly provides all the ripples. This will effectively suppress the second-order harmonic current in the front-end converter. The proposed solution, however, requires a sizeable dc-bus capacitor and induces large fluctuations of dc-bus voltage, which will have a negative effect on the inverter's output voltage quality. In [27], a current sensorless load current feedforward control scheme is proposed to mitigate the second-order harmonic component in the dc-bus voltage. In the proposed solution, instead of using a current sensor, a non-linear disturbance observer is utilized to obtain the load current. However, accurate knowledge of the converter's parameters is required for a precise estimation of the load current.

The control methods discussed earlier are based on an ideal small-signal converter model where model uncertainties and variations in converter's parameters are not taken into consideration. To address this drawback, a UDE-based dc-bus voltage control with current sensorless load current feedforward for a two-stage single-phase inverter system is proposed in this paper. The proposed control method consists of a feedforward path, a UDE, and a voltage feedback loop. The load current is estimated from the average current of the DAB's secondary bridge, and lossless sensing of the capacitor current is achieved using a digital filter. The estimated load current is fed forward to attain a fast dynamic response. However, the load current estimation accuracy and calculation of the optimum feedforward gain depends on the values of circuit parameters, which may be not known with high precision. Thus, a UDE is used to compensate for model uncertainties and parameter variations, and the voltage feedback loop is designed to ensure an excellent converter's stability. As compared to traditional single-loop voltage-mode control or voltage-mode control with load current feedforward, the proposed UDE-assisted current sensorless load current feedforward control results in an improved dynamic response performance and reduced dc-bus voltage ripple.

The organization of the rest of the paper is as follows: In Section 2, a small-signal model for a cascaded converter system consisting of a DAB dc-dc converter and a single-phase inverter is derived. A method for sensorless estimation of load current is presented in Section 3. In Section 4, a UDE is designed to compensate for converter parameter variations and model uncer-

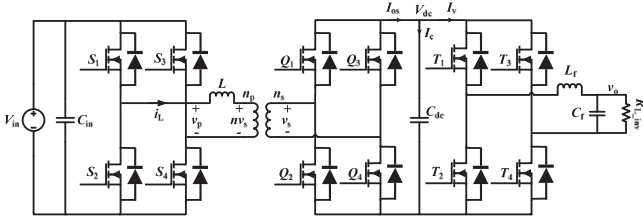


FIGURE 1 DAB converter driving an inverter load

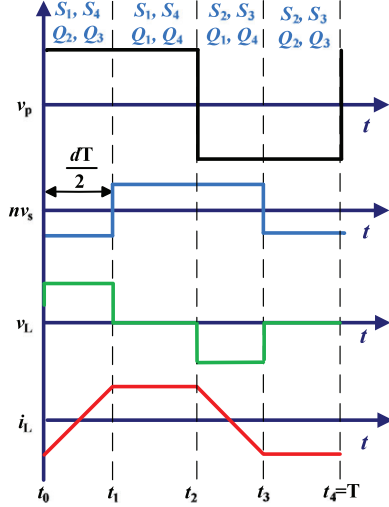


FIGURE 2 Steady-state waveforms of DAB converter with SPS modulation scheme

tainties that could lead to error in load current estimation. To validate the proposed control scheme, results obtained from the experimental prototype are given in Section 5. In Section 6, concluding remarks are given.

2 | SMALL-SIGNAL MODEL OF THE CASCADED CONVERTER SYSTEM

A cascaded two-stage system comprising the front-end DAB dc-dc converter followed by a single-phase inverter is shown in Figure 1. The DAB converter is a popular choice for most applications for front-end DC-DC power conversion stage due to its inherent advantages of soft-switching operation, symmetrical and modular structure, galvanic isolation to meet the safety requirements and bidirectional power flow capability. The most commonly used modulation method for DAB converter is the single-phase-shift modulation (SPS), where phase-shifted high-frequency square wave ac voltages (c.f., Figure 2 where v_p is the primary bridge ac voltage and v_s is the secondary bridge ac voltage) are applied across the transformers leakage inductance for power flow control. Power flows from leading to lagging ac voltage, with the phase-shift being used as a control variable to modulate the output power. The output power expression for the DAB converter controlled with SPS modulation is given by

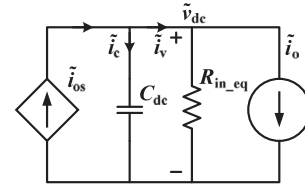


FIGURE 3 Small-signal model of DAB converter driving an inverter load

Equation (1) [28].

$$P = \frac{nV_{in}V_{dc}d(1-d)}{2f_sL}, \quad (1)$$

where V_{in} is the input voltage, V_{dc} is the dc-bus voltage, $n = \frac{n_p}{n_s}$ is the transformer's turns ratio, L is the energy transfer inductance, d is the phase-shift between v_p and v_s , and f_s is the converter switching frequency. From Equation (1), the average output current I_{os} of the DAB converter (c.f., Figure 1) is given by:

$$I_{os} = \frac{nV_{in}d(1-d)}{2f_sL}. \quad (2)$$

The small-signal variation of I_{os} , with respect to variation in d is derived by taking the partial derivative of Equation (2) with respect to d and the result is given by Equation (3):

$$G_{i_{os}d} = \frac{\tilde{i}_{os}}{\tilde{d}} = \frac{nV_{in}(1-2d)}{2f_sL}. \quad (3)$$

The DAB converter is driving a single-phase inverter that is being controlled with sinusoidal pulse width modulation. The inverter load can be modeled as an equivalent dc resistance R_{in_eq} (c.f., Equation (4)) from the UDE viewpoint, whereas the double-line frequency power fluctuation can be treated as a disturbance to be forecasted and regulated by the disturbance estimator as discussed in Section 4.

$$R_{in_eq} = \frac{V_{dc}^2 R_{L_inv}}{V_{o_rms}^2}, \quad (4)$$

where V_{dc} is the dc-bus voltage, R_{L_inv} is the inverter's load resistance, and V_{o_rms} is the rms value of the inverter's output voltage.

By inspection of Equations (3) and (4), the small-signal average model of the cascaded system (i.e. a single-phase inverter being driven by the front-end DAB converter) can be derived as illustrated in Figure 3, where C_{dc} is the dc-bus capacitor, \tilde{i}_v is the small-signal load current, \tilde{i}_{os} is the small-signal output bridge current and \tilde{i}_o is the small-signal perturbation to the load current. The open-loop small-signal output current-to-bus voltage and control-to-bus voltage transfer functions can be obtained from Figure 3 and the results are given by Equations (5) and (6),

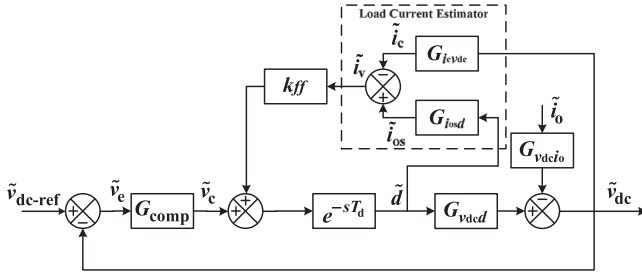


FIGURE 4 Closed-loop small-signal block diagram of DAB converter driving an inverter load with sensorless load current feedforward

respectively.

$$G_{v_{dc}d} = \frac{\tilde{v}_{dc}}{\tilde{d}} = \frac{nV_{in}R_{in_eq}(1-2d)}{2f_sL(1+sR_{in_eq}C_{dc})}, \quad (5)$$

$$G_{v_{dc}i_o} = \frac{\tilde{v}_{dc}}{-\tilde{i}_o} = \frac{R_{in_eq}}{1+sR_{in_eq}C_{dc}}. \quad (6)$$

3 | CURRENT SENSORLESS LOAD-CURRENT FEEDFORWARD

In conventional voltage-mode control, the PI controller needs to meet two crucial requirements simultaneously, that is a fast dynamic response and absolute stability, and it is challenging to optimize the design of the PI controller for achieving these objectives simultaneously with one set of design parameters. Hence, there is always a trade-off between stability and dynamic response performance when PI control is used alone. To obtain an enhanced transient response to fast load transients without affecting stability, feedforward control is an effective method. Figure 4 shows the small-signal block diagram of a DAB converter with load current feedforward. Referring to Figure 4, G_{comp} is the transfer function of the feedback compensator, e^{-sT_d} represents the delay due to digital implementation of the control algorithm, $G_{v_{dc}d}$ is the control-to-dc-bus voltage transfer function, $G_{v_{dc}i_o}$ is the load current-to-dc-bus voltage transfer function, $G_{i_{os}d}$ is the control-to-output bridge current transfer function, $G_{i_c v_{dc}}$ is the dc-bus voltage-to-capacitor current transfer function and K_{ff} is the load current feedforward gain.

From Figure 4, the closed-loop output impedance of the DAB converter (i.e. the transfer function from \tilde{i}_o to \tilde{v}_{dc}) can be derived as given by Equation (7).

$$Z_{oc} = \frac{\tilde{v}_{dc}}{-\tilde{i}_o} = \frac{G_{v_{dc}i_o}}{1 + \frac{(G_{comp} + k_{ff}G_{i_c v_{dc}})G_{v_{dc}d}e^{-sT_d}}{1 - K_{ff}G_{i_{os}d}e^{-sT_d}}}. \quad (7)$$

By setting Equation (7) equal to zero, the optimal feedforward gain can be obtained as

$$k_{ff} = \frac{1}{e^{-sT_d}G_{i_{os}d}}. \quad (8)$$

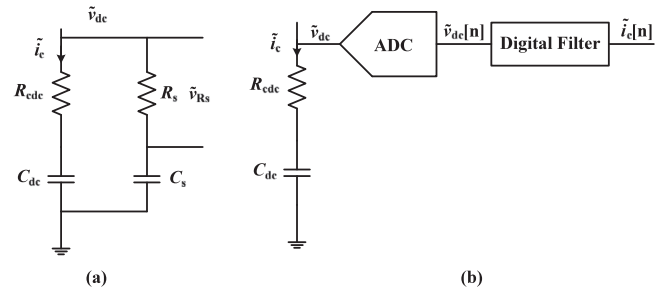


FIGURE 5 Current sensorless capacitor current sensing

Substituting the transfer functions $G_{i_{os}d}$ from Equation (3) into Equation (8), and ignoring the delay term for $\omega T_d \ll 1$, the optimal feedforward gain can be obtained as follows:

$$k_{ff} = \frac{2f_sL}{nV_{in}(1-2d)}. \quad (9)$$

It can be seen from Equation (9) that the optimal load current feedforward gain for the DAB converter requires the values of the energy transfer inductance, input voltage, and transformer turns ratio.

To implement load current feedforward control, information of the load current is required. The most direct method to obtain load current information is by using a current-sense resistor or a Hall-effect sensor. However, the former will incur additional losses while the latter will require an extra current sensor which increases cost and bulkiness. An alternative method to obtain load current information without using additional sensor, and therefore does not incur additional losses, is to estimate the load current from the output bridge's current and capacitor current according to Equation (10).

$$\tilde{i}_v = \tilde{i}_{os} - \tilde{i}_c, \quad (10)$$

where \tilde{i}_v is the average load current, \tilde{i}_c is the average capacitor current and \tilde{i}_{os} is the average output current of the DAB converter's secondary bridge and is given by Equation (3).

To estimate the capacitor current without current sensor, the method shown in Figure 5 based on the well-known impedance matching principle is applied [29, 30]. For the R_sC_s network shown in Figure 5(a), the following relationship can be obtained.

$$\tilde{v}_{RS} = \tilde{i}_c R_{cde} \left(\frac{1 + \frac{1}{sR_{cde}C_{dc}}}{1 + \frac{1}{sR_sC_s}} \right), \quad (11)$$

$$G_{i_c v_{dc}} = \frac{\tilde{i}_c}{\tilde{v}_{dc}} = \frac{1}{R_{cde} \left(1 + \frac{1}{sC_{dc}R_{cde}} \right)}. \quad (12)$$

From Equation (11), it can be deduced that if the time constant of the dc-bus capacitor matches the time constant of

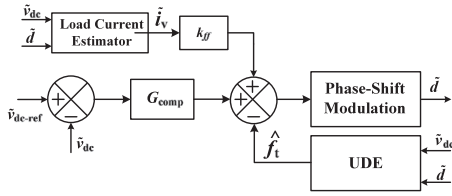


FIGURE 6 Block diagram of UDE-assisted sensorless load feedforward for dc-bus voltage regulation

the sensing network, the voltage across the sense resistor V_{RS} becomes a scaled version of the capacitor current. However, it is not practically feasible to know the time constant of the dc-bus capacitor with high precision (e.g. both capacitance and ESR are sensitive to operating temperature), and therefore, such a current sense method is always prone to error. This error is estimated and compensated by an UDE which is used to enhance the robustness of the proposed control scheme, and its design and implementation will be discussed in the next section.

In digital implementation, the analog $R_s C_s$ filter is replaced by a digital filter as shown in Figure 5(b) and the dc-bus voltage is sensed and passed through a digital filter having a time constant equal to that of the dc-bus capacitor. By applying bilinear-transformation to Equation (12), the “sensed” capacitor current can be expressed as follows:

$$\tilde{i}_c[n] = C_1 \tilde{i}_c[n-1] + C_2 (\tilde{v}_{dc}[n] - \tilde{v}_{dc}[n-1]), \quad (13)$$

with

$$C_1 = \frac{(2R_{dc} C_{dc} - T_s)}{(2R_{dc} C_{dc} + T_s)} \quad C_2 = \frac{2C_{dc}}{(2R_{dc} C_{dc} + T_s)}.$$

4 | UDE-ASSISTED SENSORLESS LOAD-CURRENT FEEDFORWARD FOR DC-BUS VOLTAGE REGULATION

The performance of load current feedforward control is expected to be optimal when the feedforward gain is optimal and the “sensed” load current information is accurate. However, the optimality of the selected feedforward gain is not always guaranteed due to parameter variations and model uncertainties such as the effects of un-modelled parasitic components. For this reason, in this work, an UDE-assisted sensorless load current feedforward control method for DAB converter driving an inverter is proposed to enhance the DAB converter’s dynamic response performance and mitigate the second-order harmonic component in the dc-bus voltage. The block diagram of the proposed UDE-assisted sensorless load current feedforward control is shown in Figure 6 where the load current is estimated using Equations (10) and (13), and a feedforward control signal is added to the output of the voltage loop’s feedback compensator. In addition to this, the total lumped disturbance due to converter parameter variations and model uncertainties are estimated utilizing a UDE with the aim to achieve a robust

and tight control of the dc-bus voltage. From Figure 3, by using Kirchhoff’s current law, the dc-bus capacitor dynamics can be expressed as follows:

$$\frac{d\tilde{v}_{dc}}{dt} = -\frac{\tilde{v}_{dc}}{R_{in_eq} C_{dc}} + \frac{nV_{in}(1-2d)}{2f_s LC_{dc}} \tilde{d}, \quad (14)$$

which can be rearranged as Equation (15)

$$\dot{\tilde{v}}_{dc} = a\tilde{v}_{dc} + b\tilde{d}, \quad (15)$$

where

$$a = -\frac{1}{R_{in_eq} C_{dc}} \quad b = \frac{nV_{in}(1-2d)}{2f_s LC_{dc}}.$$

Equation (15) can be amended to include the effects of disturbance by adding a lumped disturbance term f_t .

$$\dot{\tilde{v}}_{dc} = a\tilde{v}_{dc} + b\tilde{d} + f_t, \quad (16)$$

where $f_t = \Delta a\tilde{v}_{dc} + \Delta b\tilde{d}$. Hence, the total lumped uncertainty and disturbance can be estimated from Equation (16) as follows [31, 32]:

$$f_t = \dot{\tilde{v}}_{dc} - a\tilde{v}_{dc} - b\tilde{d}. \quad (17)$$

However, the derivative state variable $\dot{\tilde{v}}_{dc}$ cannot be measured directly, hence it is estimated using an UDE represented by Equation (18).

$$\hat{f}_t = f_t \star g_f, \quad (18)$$

where \star is the convolution operator and g_f is the impulse response of a low-pass filter $G_f(s)$ given by Equation (19).

$$G_f(s) = \frac{1}{1 + \frac{s}{\omega_{fc}}}. \quad (19)$$

Taking the Laplace transform of Equation (18) gives

$$\hat{f}_t(s) = \left(\frac{s-a}{1 + \frac{s}{\omega_{fc}}} \right) \tilde{v}_{dc} - \left(\frac{b}{1 + \frac{s}{\omega_{fc}}} \right) \tilde{d} = G_{fv_{dc}} \tilde{v}_{dc} - G_{fd} \tilde{d}. \quad (20)$$

Based on Equation (20), the small-signal block diagram of the DAB converter with UDE-assisted sensorless load current feedforward control is shown in Figure 7.

4.1 | Feedback controller design

The feedback controller of the DAB converter is designed in frequency domain in this section. The UDE estimates the total lumped disturbances by using the sensed dc-bus voltage \tilde{v}_{dc} and

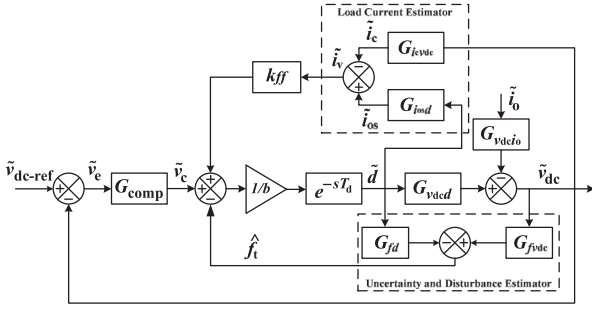


FIGURE 7 Closed-loop small-signal block diagram of DAB converter driving an inverter load with UDE-assisted sensorless load current feedforward

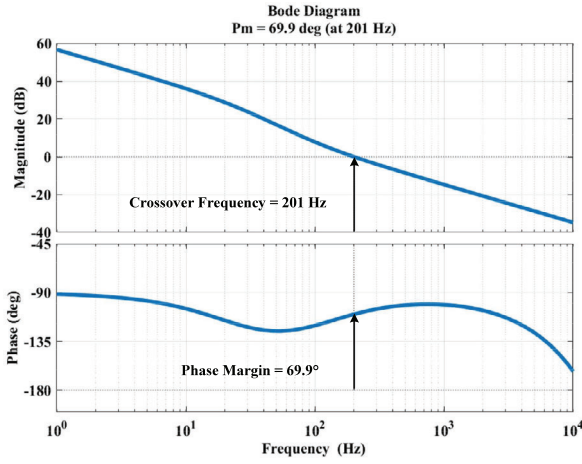


FIGURE 8 Bode plot of converter's loop gain with UDE-assisted sensorless load current feedforward control

the phase-shift \tilde{d} as inputs. From Equation (20), the s -domain transfer function from the compensated error signal \tilde{d} to the total lumped disturbances \hat{f}_t and from the dc-bus voltage \tilde{v}_{dc} to the total lumped disturbances \hat{f}_t can be derived as given by Equations (21) and (22), respectively. From the small-signal control block diagram of the DAB converter depicted in Figure 7,

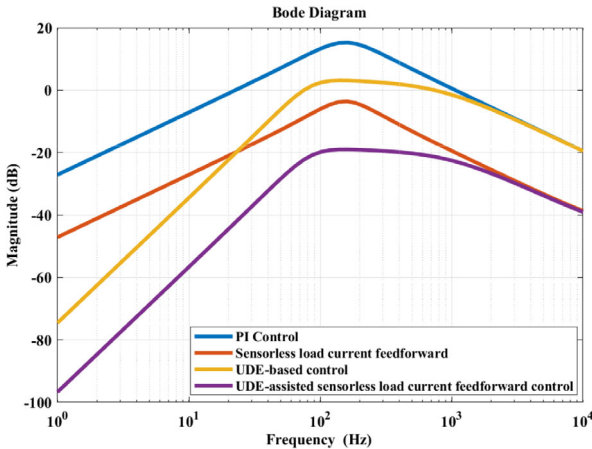


FIGURE 9 Closed-loop output impedance of DAB converter under different control schemes

TABLE 1 Specifications of experimental prototype

DAB converter	
Input voltage V_{in}	200 V
DC-bus voltage V_{dc}	100 V
Rated output power P_o	250 W
Switching frequency f_s	50 kHz
Turns ratio n	2 : 1
Inductance L	160 μ H
DC-bus electrolytic capacitor	150 μ F
Load resistor	40 Ω
Controller	TI TMS320F28379D
Inverter	
Output voltage V_o	50 V _{rms}
Modulator frequency f_m	50 Hz
Carrier frequency f_c	50 kHz
Filter inductor L_f	500 μ H
Filter capacitor C_f	20 μ F
Load resistor	10 Ω

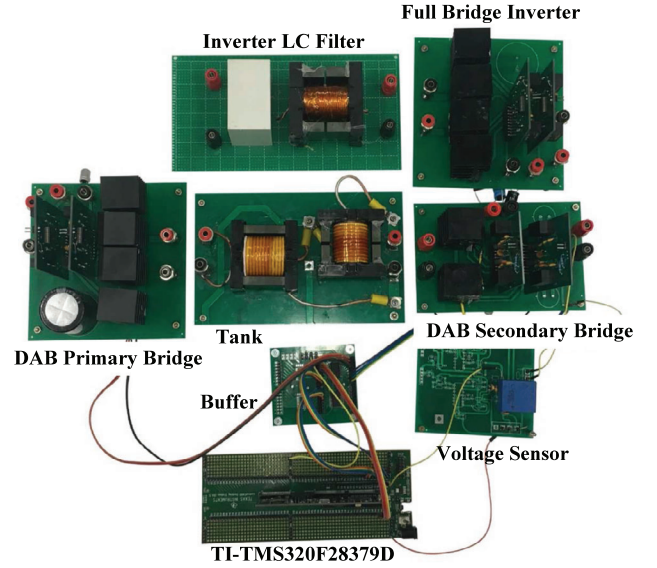
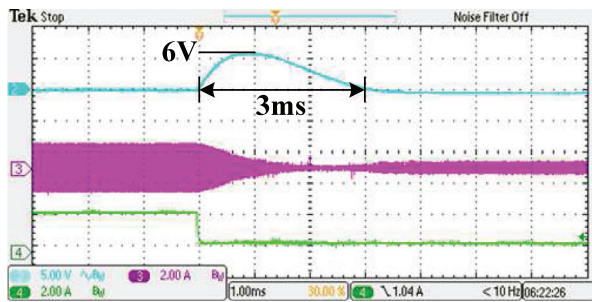


FIGURE 10 Hardware prototype of a DAB converter and single-phase inverter

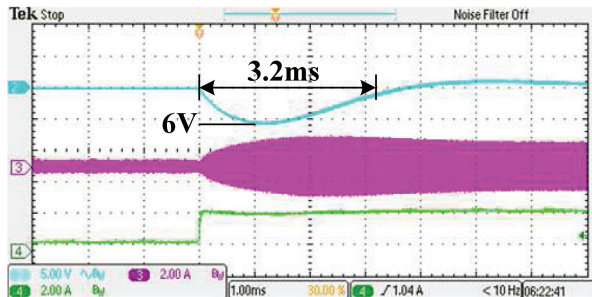
the transfer function from the compensated error signal \tilde{v}_c to the dc-bus voltage \tilde{v}_{dc} is given by Equation (23).

$$G_{fd} = \frac{\hat{f}_t}{\tilde{d}} = \frac{b}{1 + \frac{s}{\omega_{fc}}}, \quad (21)$$

$$G_{f\tilde{v}_{dc}} = \frac{\hat{f}_t}{\tilde{v}_{dc}} = \frac{s - a}{1 + \frac{s}{\omega_{fc}}}, \quad (22)$$



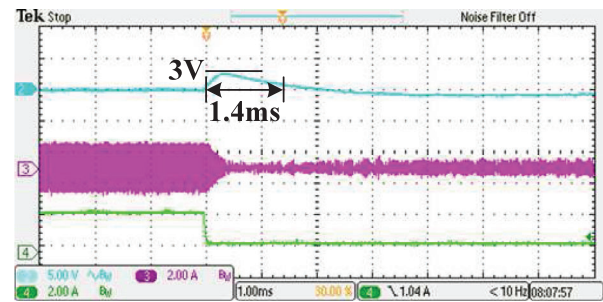
(a)



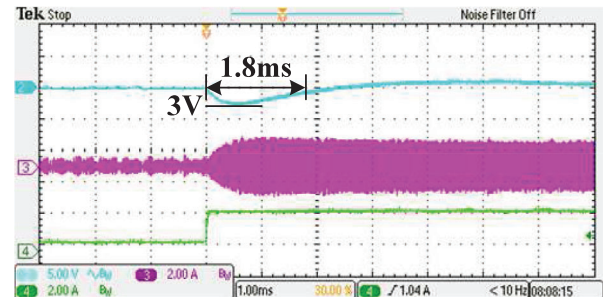
(b)

Time: 1ms/Div.
Top Trace (DC-bus Voltage, AC Coupled): 5V/Div.
Middle Trace (Inductor Current): 2A/Div.
Bottom Trace (Load Current): 2A/Div.

FIGURE 11 Step response of DAB converter with PI control



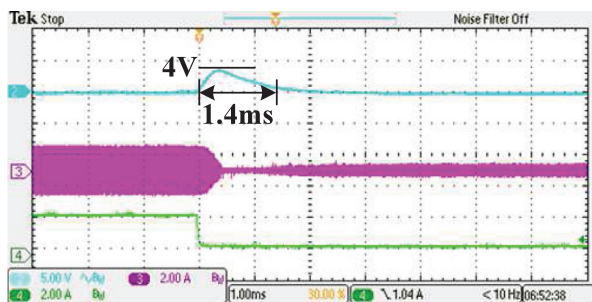
(a)



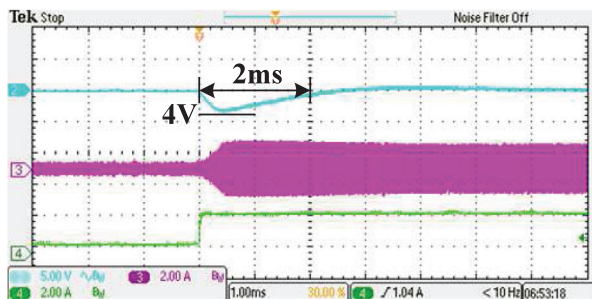
(b)

Time: 1ms/Div.
Top Trace (DC-bus Voltage, AC Coupled): 5V/Div.
Middle Trace (Inductor Current): 2A/Div.
Bottom Trace (Load Current): 2A/Div.

FIGURE 13 Step response of DAB converter with UDE-based control only



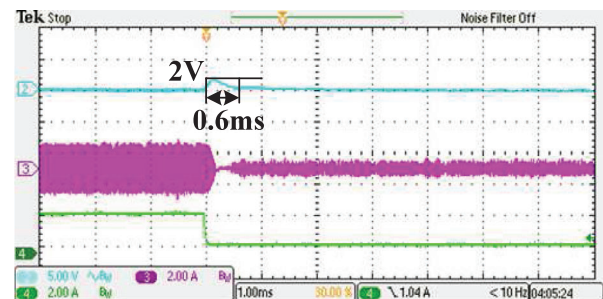
(a)



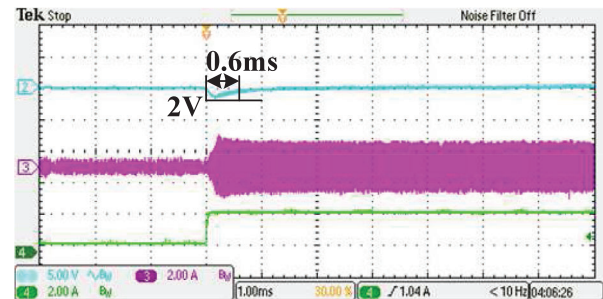
(b)

Time: 1ms/Div.
Top Trace (DC-bus Voltage, AC Coupled): 5V/Div.
Middle Trace (Inductor Current): 2A/Div.
Bottom Trace (Load Current): 2A/Div.

FIGURE 12 Step response of DAB converter with sensorless load current feedforward



(a)



(b)

Time: 1ms/Div.
Top Trace (DC-bus Voltage, AC Coupled): 5V/Div.
Middle Trace (Inductor Current): 2A/Div.
Bottom Trace (Load Current): 2A/Div.

FIGURE 14 Step response of DAB converter with UDE-assisted sensorless load current feedforward control

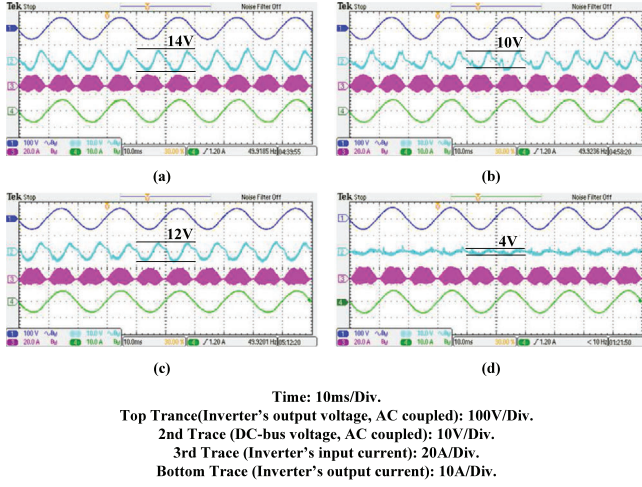


FIGURE 15 Steady-state experimental waveforms of DAB converter driving a single-phase inverter: (a) PI control; (b) sensorless load current feedforward; (c) UDE-based control; (d) UDE-assisted sensorless load current feedforward

$$G_{v_{dc}v_c} = \frac{\tilde{v}_{dc}}{\tilde{v}_c} = \frac{G_{v_{dc}d} b^{-1} e^{-sT_d}}{1 + G_{v_{dc}d} b^{-1} e^{-sT_d} (G_{fd} G_{v_{dc}d}^{-1} + G_{fv_{dc}})}. \quad (23)$$

Substituting the transfer functions G_{fd} and $G_{fv_{dc}}$ from Equations (21) and (22) into Equation (23) gives

$$G_{v_{dc}v_c} = \frac{\tilde{v}_{dc}}{\tilde{v}_c} = \frac{G_{v_{dc}d} b^{-1} e^{-sT_d}}{1 - \frac{e^{-sT_d}}{1 + \frac{s}{\omega_{fc}}} + \frac{(s-a)}{1 + \frac{s}{\omega_{fc}}} (G_{v_{dc}d} b^{-1} e^{-sT_d})}. \quad (24)$$

For $\omega \ll \omega_{fc}$, Equation (24) can be approximated as follows (ω_{fc} is selected to be 5 times of the compensated loop gain's crossover frequency):

$$G_{v_{dc}v_c} = \frac{\tilde{v}_{dc}}{\tilde{v}_c} \approx \frac{1}{s-a}. \quad (25)$$

From Equation (25), it can be concluded that the modified plant has a dominant pole open-loop characteristics; thus, a simple PI controller can be used to obtain the desired phase margin and zero steady-state error. Figure 8 shows the compensated loop-gain with a phase margin of 69° and a crossover frequency of 200Hz.

4.2 | Closed-loop output impedance

In this section, the effect of the UDE-assisted sensorless load current feedforward control on the closed-loop output impedance of the DAB converter is investigated. From Figure 7, the closed-loop output impedance of the DAB converter's can be derived as given by Equation (26). Figure 9 shows the calculated closed-loop output impedance of the DAB converter under different control schemes. For a fair comparison, the

same PI controller's parameters are used in all cases. From the figure, it can be seen that with the proposed control scheme, the DAB converter's closed-loop output impedance has been attenuated significantly and is consistently the lowest at all frequencies among all the control schemes considered. Next, the proposed control scheme is validated experimentally on hardware prototype.

$$Z_{ocl} = \frac{\tilde{v}_{dc}}{-\tilde{i}_o} = \frac{G_{v_{dc}i_o}}{1 + \frac{(G_{comp} + G_{fv_{dc}} + G_{icv_{dc}} k_{ff}) G_{v_{dc}d} e^{-sT_d}}{b + G_{fd} e^{-sT_d} - G_{iosd} k_{ff} e^{-sT_d}}}. \quad (26)$$

5 | EXPERIMENTAL RESULTS

The proposed control scheme is implemented on a DAB dc-dc converter in two different configurations to validate its effectiveness, that is, the DAB converter is terminated with a resistive load which is then replaced by a single-phase inverter. The nominal parameters of experimental prototypes are listed in Table 1. The control algorithm is implemented digitally on a digital signal processor (DSP) TMS320F28339D. The DSP has an on-chip analog-to-digital (ADC) and a pulse-width modulator (PWM). An analog voltage sensor is utilized to measure dc-bus voltage which is then sampled and is converted to a digital output by the use of an on-chip ADC of the DSP controller. The control algorithm is then executed at a fixed frequency in the interrupt service routine. Based on the output of the control algorithm, the on-chip PWM module is used to generate the control signals for the switching devices of the DAB converter and single-phase inverter.

5.1 | Dynamic performance to step load change

Figure 11(a,b) represents the load step dynamic responses of the DAB converter (terminated with resistive load) when the voltage V_{dc} at the dc-bus is regulated by using a well-tuned PI controller. The maximum overshoot and undershoot of the V_{dc} is approximately 6 V and a settling time of 3 ms when step load changes of $0.5A \leftrightarrow 2.5A$ were applied. Moreover, the dynamic response of the DAB converter to similar load step changes with sensorless load current feedforward control only is shown in Figure 12, where the maximum overshoot and undershoot of the dc-bus voltage is reduced to 4 V and the settling time is decreased to 2 ms. Figure 13 represents the dynamic response of the DAB converter when V_{dc} is regulated by UDE-based control alone (i.e. without load current feedforward) and it can be seen that dynamic response is improved as compared to that of the previous two cases in term of voltage overshoot/undershoot and settling time.

Figure 14 shows a further improvement in the dynamic response when UDE-based control is combined with current sensorless load current feedforward as shown in . The

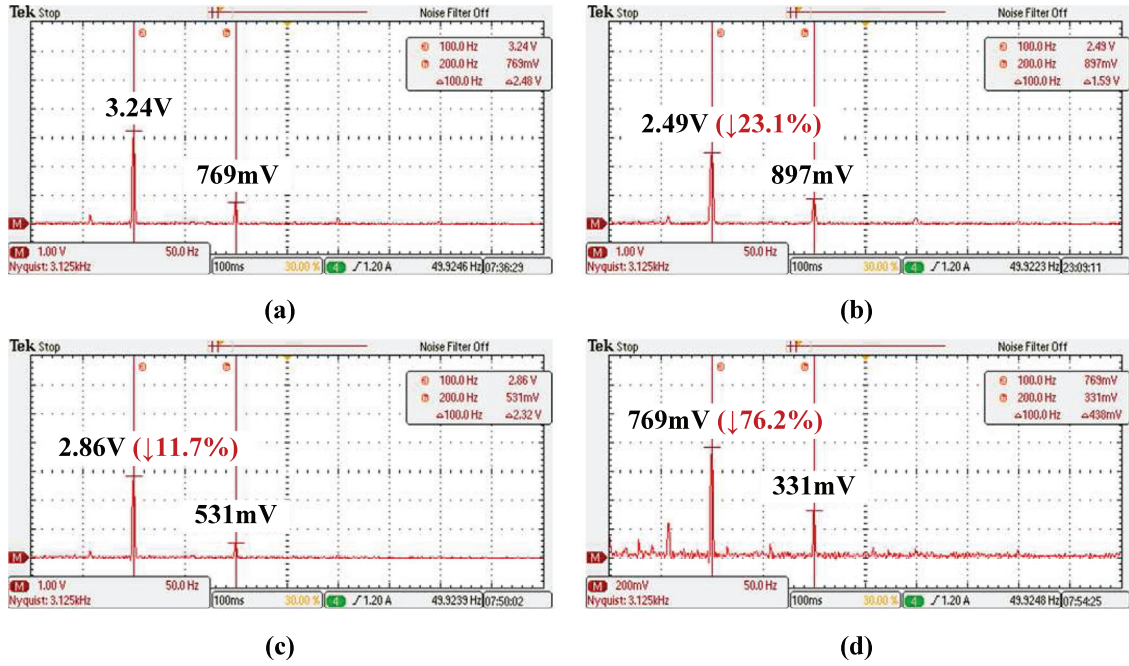


FIGURE 16 FFT spectrum of DAB converter's dc-bus voltage V_{dc} : (a) PI control; (b) sensorless load current feedforward; (c) UDE-based control; (d) UDE-assisted sensorless load current feedforward

maximum overshoot and undershoot of the dc-bus voltage is reduced to 2 V with a settling time of only 0.6 ms, or 1/5 of that resulted from PI control. From these results, it can be concluded that the DAB converter has the most sluggish dynamic response performance when the V_{dc} is regulated by using conventional PI control. The DAB converter exhibits improved dynamic response when either or both of the sensorless load current feedforward control and UDE-based control are implemented. However, the best dynamic response performance is exhibited by the combined effect of these two control schemes. The reasons for this is that any non-idealities that may affect the effectiveness of load current feedforward control are compensated in large part by the compensative actions of the UDE, making it approach the performance of an optimal feedforward controller.

5.2 | Dynamic performance of DAB converter driving a single-phase inverter

Figure 15 represents the steady-state waveforms of the DAB converter driving a single-phase inverter. The first trace shows the inverter's output voltage v_o , the second trace shows the dc-bus voltage V_{dc} , the third trace is the inverter's input current I_v , (i.e. DAB converter's output current), and the fourth trace is the inverter's output current i_o . It can be observed from Figure 15a that regulating V_{dc} by using PI controller leads to a large double-line frequency component present in the V_{dc} . Figures 15(b) and 15(c) show that the dc-bus voltage ripple has been reduced (by 28.6% and 14.3% respectively) when the V_{dc} is regulated using sensorless load current feedforward or UDE-

based control. When sensorless load current feedforward control is enhanced by the UDE as shown in Figure 15(d), V_{dc} ripple is further reduced by 60%–66.7% giving a smooth dc-bus voltage.

The reduction in the dc-bus voltage V_{dc} ripple and its effect on the inverter's output voltage v_o can be more distinctively visualized from the Fast-Fourier-Transform (FFT) spectrum of V_{dc} and v_o . Figures 16 and 17 represent the FFT spectrum of the V_{dc} and v_o under different control schemes. It can be seen from Figure 16(a) that, when the V_{dc} is regulated using PI control, there is a large double-line frequency ripple component in the V_{dc} leading to a large third-order harmonic component in the inverter's output voltage due to the intermodulation between the inverter's fundamental frequency (50 Hz) and the double-line frequency present in V_{dc} , as evident from Figure 17(a). On the other hand, when the V_{dc} is regulated by UDE-assisted sensorless load current feedforward, the double-line frequency ripple component on the V_{dc} is significantly attenuated which results in a decrement of the third-order harmonic component in the v_o , and thus improved inverter's output voltage quality.

6 | CONCLUSION

This paper proposes a new sensorless load current feedforward control method to achieve improved dc-bus voltage regulation in a cascaded converter system comprising a DAB dc-dc front-end converter and a single-phase inverter. Without using sensor, the load current is estimated from the calculated DAB's output bridge current and lossless sensing (with digital filter) of the dc-bus capacitor current. The effects of any non-idealities on

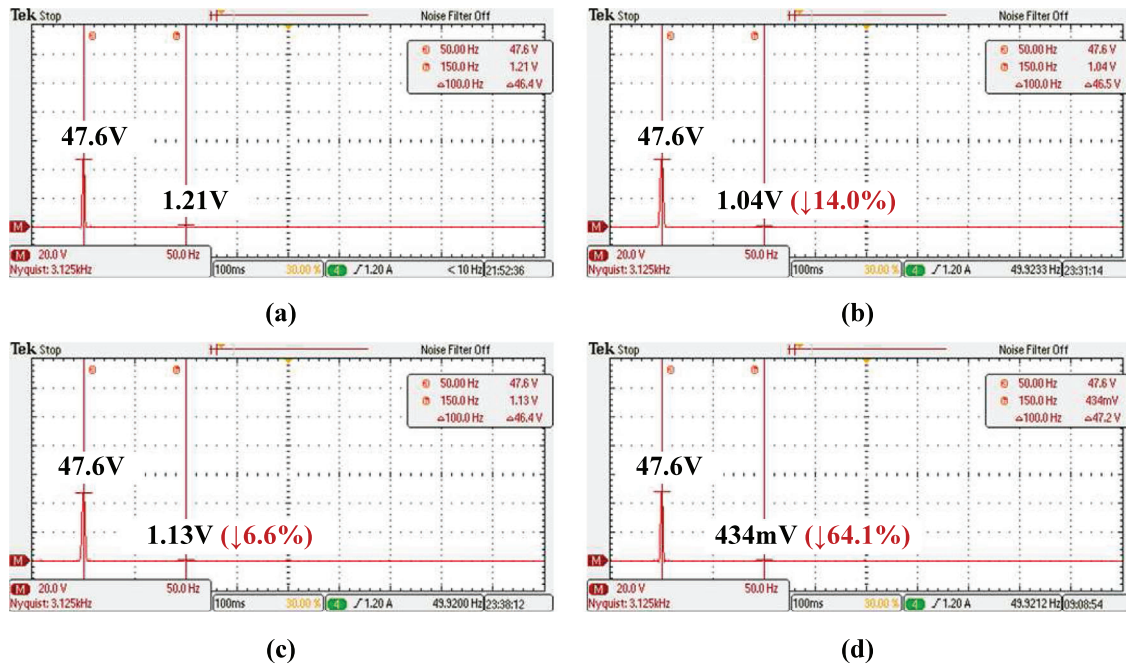


FIGURE 17 FFT spectrum of single-phase inverter's output voltage v_o : (a) PI control; (b) sensorless load current feedforward; (c) UDE-based control; (d) UDE-assisted sensorless load current feedforward

load current estimation are compensated by an UDE, thus making the proposed control scheme robust against uncertainties in circuit parameters and other un-modeled effects. It has been verified experimentally that the dynamic response performance of the DAB dc-dc converter has been significantly enhanced by the proposed control scheme in comparison with conventional PI control and the case when load current feedforward or UDE-based control is used alone. When subjected to step load change, it has led to 66.7% reduction in output voltage overshoot/undershoot and 80% reduction in settling time compared to conventional PI control. When cascaded with a single-phase inverter, the double-line frequency ripple component in the dc-bus voltage is reduced by 76.2% compared to conventional PI control, confirming the effectiveness of the proposed control scheme.

ACKNOWLEDGEMENT

This work was supported by The Hong Kong Polytechnic University Central Research Grant G-YBXL.

ORCID

Majid Ali  <https://orcid.org/0000-0003-0153-3645>

REFERENCES

- Zhang, H., et al.: Observer-pattern modeling and nonlinear modal analysis of two-stage boost inverter. *IEEE Trans. Power Electron.* 33(8), 6822–6836 (2018)
- Kim, J.S., Kwon, J.M., Kwon, B.H.: High-efficiency two-stage three-level grid-connected photovoltaic inverter. *IEEE Trans. Ind. Electron.* 65(3), 2368–2377 (2018)
- Ye, Q., Mo, R., Li, H.: Low-frequency resonance suppression of a dual-active-bridge dc/dc converter enabled dc microgrid. *IEEE J. Emerging Sel. Top. Power Electron.* 5(3), 982–994 (2017)
- Zakzouk, N.E., et al.: PV single-phase grid-connected converter: dc-link voltage sensorless prospective. *IEEE J. Emerging Sel. Top. Power Electron.* 5(1), 526–546 (2017)
- Yaqoob, M., Loo, K.H., Lai, Y.M.: Fully soft-switched dual-active-bridge series-resonant converter with switched-impedance-based power control. *IEEE Trans. Power Electron.* 33(11), 9267–9281 (2018)
- De Din, E., et al.: Voltage control of parallel-connected dual-active bridge converters for shipboard applications. *IEEE J. Emerging Sel. Top. Power Electron.* 6(2), 664–673 (2018)
- Xu, G., et al.: Dual-transformer-based DAB converter with wide ZVS range for wide voltage conversion. *IEEE Trans. Ind. Electron.* 65(4), 3306–3316 (2018)
- Irfan, M.S., et al.: Current-sensorless power-decoupling phase-shift dual-half-bridge converter for DC-AC power conversion systems without electrolytic capacitor. *IEEE Trans. Power Electron.* 32(5), 3610–3622 (2017)
- Zhu, G.R., et al.: Enhanced single-phase full-bridge inverter with minimal low-frequency current ripple. *IEEE Trans. Ind. Electron.* 63(2), 937–943 (2016)
- Cao, X., Zhong, Q.C., Ming, W.L.: Ripple eliminator to smooth dc-bus voltage and reduce the total capacitance required. *IEEE Trans. Ind. Electron.* 62(4), 2224–2235 (2015)
- Agamy, M.S., et al.: A high power medium voltage resonant dual active bridge for MVDC ship power networks. *IEEE J. Emerging Sel. Top. Power Electron.* 5(1), 88–99 (2017)
- Krismser, F., Kolar, J.W.: Accurate small-signal model for the digital control of an automotive bidirectional dual active bridge. *IEEE Trans. Power Electron.* 24(12), 2756–2768 (2009)
- Segaran, D., Holmes, D.G., McGrath, B.P.: Enhanced load step response for a bidirectional DC-DC converter. *IEEE Trans. Power Electron.* 28(1), 371–379 (2013)
- Shan, Z., et al.: Simplified load-feedforward control design for dual-active-bridge converters with current-mode modulation. *IEEE J. Emerging Sel. Top. Power Electron.* 6(4), 2073–2085 (2018)
- Oggier, G.G., et al.: Fast transient boundary control and steady-state operation of the dual active bridge converter using the natural switching surface. *IEEE Trans. Power Electron.* 29(2), 946–957 (2014)
- Dutta, S., Hazra, S., Bhattacharya, S.: A digital predictive current-mode controller for a single-phase high-frequency transformer-isolated

- dual-active bridge DC-to-DC converter. *IEEE Trans. Ind. Electron.* 63(9), 5943–5952 (2016)
17. Li, X., et al.: Asymmetric-double-sided modulation for fast load transition in a semi-dual-active-bridge converter. *IET Power Electron.* 10(13), 1698–1704 (2017)
 18. Aboushady, A.A., et al.: Lyapunov-based high-performance controller for modular resonant dc/dc converters for medium-voltage dc grids. *IET Power Electron.* 10(15), 2055–2064 (2017)
 19. Nguyen, D.D., et al.: Reduced-order observer-based control system for dual-active-bridge DC/DC converter. *IEEE Trans. Ind. Appl.* 54(4), 3426–3439 (2018)
 20. Song, W., Hou, N., Wu, M.: Virtual direct power control scheme of dual active bridge DC-DC converters for fast dynamic response. *IEEE Trans. Power Electron.* 33(2), 1750–1759 (2018)
 21. Hou, N., et al.: A comprehensive optimization control of dual active bridge DC-DC converters based on unified-phase-shift and power-balancing scheme. *IEEE Trans. Power Electron.* 34(1), 826–839 (2019)
 22. Qin, H., Kimball, J.W.: Closed-loop control of DC-DC dual-active-bridge converters driving single-phase inverters. *IEEE Trans. Power Electron.* 29(2), 1006–1017 (2014)
 23. Zhang, L., Ren, X., Ruan, X.: A bandpass filter incorporated into the inductor current feedback path for improving dynamic performance of the front-end DC-DC converter in two-stage inverter. *IEEE Trans. Ind. Electron.* 61(5), 2316–2325 (2014)
 24. Cao, L., Loo, K.H., Lai, Y.M.: Systematic derivation of a family of output-impedance shaping methods for power converters - a case study using fuel cell-battery-powered single-phase inverter system. *IEEE Trans. Power Electron.* 30(10), 5854–5869 (2015)
 25. Cao, L., Loo, K.H., Lai, Y.M.: Output-impedance shaping of bidirectional DAB DC-DC converter using double-proportional-integral feedback for near-ripple-free DC bus voltage regulation in renewable energy systems. *IEEE Trans. Power Electron.* 31(3), 2187–2199 (2016)
 26. Shi, Y., Liu, B., Duan, S.: Low-frequency input current ripple reduction based on load current feedforward in a two-stage single-phase inverter. *IEEE Trans. Power Electron.* 31(11), 7972–7985 (2016)
 27. Xiong, F., et al.: Current sensorless control for dual active bridge DC-DC converter with estimated load-current feedforward. *IEEE Trans. Power Electron.* 33(4), 3552–3566 (2018)
 28. Rodriguez, A., et al.: Different purpose design strategies and techniques to improve the performance of a dual active bridge with phase-shift control. *IEEE Trans. Power Electron.* 30(2), 790–804 (2015)
 29. Simón.Muela, A., et al.: Practical implementation of a high-frequency current-sense technique for VRM. *IEEE Trans. Ind. Electron.* 55(9), 3221–3230 (2008)
 30. Lukić, Z., et al.: Sensorless self-tuning digital CPM controller with multiple parameter estimation and thermal stress equalization. *IEEE Trans. Power Electron.* 26(12), 3948–3963 (2011)
 31. Chen, W.H., et al.: Disturbance-observer-based control and related methods - an overview. *IEEE Trans. Ind. Electron.* 63(2), 1083–1095 (2016)
 32. Han, J.: From PID to active disturbance rejection control. *IEEE Trans. Ind. Electron.* 56(3), 900–906 (2009)

How to cite this article: Ali M, Yaqoob M, Cao L, Loo K-H. Enhancement of DC-bus voltage regulation in cascaded converter system by a new sensorless load current feedforward control scheme. *IET Power Electron.* 2021;14:1457–1467.

<https://doi.org/10.1049/pel2.12123>